Enhancement of the Optoelectric and Photovoltaic Responses of Al/PVP:ZnTiO₃/p-Si Structure by Graphene Nanoparticles

Ali Barkhordari,* Şemsettin Altındal, Süleyman Özçelik, Hamid Reza Mashayekhi, Mustafa Muradov, and Yashar Azizian-Kalandaragh

In this work, the optoelectronic response of Al/p-Si photodiodes (PDs) with and without (PVP:Gr-ZnTiO₃) composite interlayer is investigated in dark and under various light intensities (P). The manufacturing/surface preparation is thoroughly explained. The electric/optic parameters including leakage/saturation current (I_0), series/shunt resistances (R_s/R_{sh}), barrier height (BH), ideality factor (n), energy-dependent density distribution of surface/interface levels (N_{ss}), photoinduced current (I_{ph}), photosensitivity (S), optical responsivity (R), and specific detectivity (D^*) are calculated from the I–V data in dark and under illumination intensities. Raising the light intensity results in a drop in Φ_{B0} and R_s quantities while increasing the I_0 and n values due to photogenerated electron–hole pairs under illumination. The Φ_{B0}-P and Φ_{B0}-n graphs are used to calculate the illumination factor and the Φ_{B0} in the ideal form. An acceptable linear behavior appears in the I_{ph}–P profiles for the negative-bias region, where the illumination dependence of photocurrent is explored. It is found that the (PVP: Gr-ZnTiO₃) interlayer leads to an increase in the S, R, and D^* values of the PD to ≈1200, 400 mA W^{-1}, and 1.14×10^{14} Jones, respectively. These results show that the used (PVP:ZnTiO₃) interlayer displays an excellent photoresponse and may effectively replace conventional PDs for applications in optoelectronic and photovoltaic devices.

1. Introduction

Direct conversion of solar radiation to direct current (DC) electricity is made possible by the photovoltaic effect in solar cells (SCs), photodiodes (PDs), and photodetectors. In order to accomplish this conversion, an absorbent material that permits the passage of these high-energy electrons through an external circuit is required. The form of the barrier height at the metal–semiconductor (MS) interface, series resistances (R_s), applied bias voltage, surface contamination, surface/interface states density distributions (N_{ss}), surface and fabrication preparations, and other factors all affect the optical characteristics and charge or current transport/conduction mechanisms (CTMs, CCMs) into the aforementioned instruments.[1–3] Historically, the fundamental scientific and technical issues with these instruments have also been connected to improving efficiency and lowering cost and energy losses. Consequently, a great deal of research has been done on organic silicon-based electronic structures, which have long been a viable substitute for inorganic silicon-based electronic structures in many ways.[3,4] It has been demonstrated that among the most appropriate possibilities for

A. Barkhordari, H. R. Mashayekhi
Faculty of Physics
Shahid Bahonar University of Kerman
Kerman 76131, Iran
E-mail: alibarkhordari20@gmail.com

Ş. Altındal
Department of Physics, Faculty of Sciences
Gazi University
06500 Ankara, Türkiye

ⓘ The ORCID identification number(s) for the author(s) of this article can be found under https://doi.org/10.1002/adpr.202400171.

S. Özçelik, Y. Azizian-Kalandaragh
Department of Photonics, Faculty of Applied Sciences
Gazi University
06500 Ankara, Türkiye

S. Özçelik, Y. Azizian-Kalandaragh
Photonics Application and Research Center
Gazi University
06500 Ankara, Türkiye

M. Muradov
Department of Physics, Nanocenter
Baku State University
Z. Khalilov 2, Baku Az1148, Azerbaijan

Y. Azizian-Kalandaragh
Department of Physics
University of Mohaghegh Ardabili
Ardabil 56131, Iran

**ADVANCED
SCIENCE NEWS**

www.advancedsciencenews.com

**ADVANCED
PHOTONICS
RESEARCH**

www.adpr-journal.com

organic configurations interlaid at the MS contact are polymers. Their controlled mechanical and electrical characteristics, simplicity of manufacturing in optoelectronics and electronics devices, and commercial availability are some of the advantages that set them apart from inorganic structures.[5–7] Organic polymers' structural properties also make major advancements in flexible electronics applications, like curved imaging and wearable technology, possible.[7–9] Polymers have a long history of being used as insulating interfaces in Schottky systems. Because of their excellent transparency and previously described qualities, they are commonly employed in organic SCs and PDs.[10] In today's steadily evolving optoelectronic applications, it may be argued that it is frequently favored.[11–13] In these studies, polymers have been employed as interfaces either in their pure form or doped with different nanoparticles (metals, metal oxides, graphene, graphene oxide, etc.) and even materials bound by cations and anion bonds.[14,15]

It must be noted that surface contamination and the interface density of states are known to play critical roles in the performance of PDs, particularly in semiconductor-based devices. Contaminants at the surface can introduce unwanted trap states and degrade charge transport, while high-interface state densities can lead to increased recombination rates, reducing the efficiency of charge carrier collection. Various methods have been explored to mitigate these effects, such as passivation layers, surface treatments, and careful control of the deposition environment. Passivation, for instance, has been shown to significantly reduce surface trap states, improving both the stability and performance of photodiodes. To ensure reliable performance and accurate characterization, it is crucial to implement strategies that minimize surface contamination and control interface quality.[16,17]

The considerable effects and range of applications provided by these two wideband semiconductors, namely ZnO and TiO_2, have drawn significant interest to both single materials and ZnO–TiO_2 composites.[18] ZnO has drawn interest in the literature due to its unique properties and applications in see-through electronics, chemical sensing devices, spintronics, piezoelectric devices, and ultraviolet (UV) light emitters.[19–22] When compared to semiconductors that are frequently utilized for blue–green light-emitting diode devices, such as ZnSe and GaN, ZnO stands out due to its large exciton binding energy of 60 meV.[23] On the other hand, TiO_2 is an inexpensive, nontoxic semiconductor that remains stable in aqueous conditions. The good photocatalytic qualities of TiO_2 have also been attributed to its wide bandgap and the long lifespan of photogenerated electrons and holes.[24] A comparatively considerable rate of electron–hole recombination commonly occurs in TiO_2 material.[25] ZnO doping can overcome these issues and increase the TiO_2 photoreactivity.[26] Within the ZnO–TiO_2 system, there are several different compounds, including Zinc titanate ($ZnTiO_3$, with cubic and hexagonal configurations), Zn_2TiO_4 (with cubic configuration), and $Zn_2Ti_3O_8$ (with cubic configuration).[27,28] The oxide structure of $ZnTiO_3$ in perovskite form has multiple applications, including microwave resonators,[29] gas sensors[30] (for CO, NO, CH_3CH_2OH, and others), metal–air barriers,[31] high-efficacy catalysts[32] for CO and NO reduction,[33] paint pigment,[34] and total oxidation of hydrocarbons.[35,36]

It is necessary to note that one layer of hexagonal carbon makes up the 2D structure known as graphene, which possesses remarkable mechanical, optical, and density/mobility qualities.[37] As a result, it is seen to be an excellent choice to replace Si in photonic/electrical devices.[38] A 3D bulk of graphite is formed when single layers of graphene are stacked on top of one another; the van der Waals force holds the plates together, and the spacing between them is around 0.335 nm.[38] Another great polymer that is utilized to create metal–polymer–semiconductor (MPS)-type schottky diode (SD) is polyvinylpyrrolidone (PVP), which can be made fast and cheap, has good stability, appropriate conductivity, and no harmful side effects.[39] The physicochemical processes that underlie the inclination for polymers and/or doped polymers as an active medium or interface in photovoltaic instruments mostly stem from the photogeneration of e^-–h^+ pairs, which depends on the energy directed onto the device's surface.[40,41] Furthermore, although there are few, research has been done on the use of polymer/copolymer nanocomposition in such devices.[42,43] To produce adequate photocurrent in terms of intensity and/or wavelength of the light is the primary goal of a photovoltaic construction, regardless of the layer deposition process or interface material selected.[44] At reverse bias voltages, an analogous orientation may be seen in the internal and external electric fields, contingent upon the applied voltage.[42] As a result, compared to the forward bias voltage, the total electric field in this scenario is stronger. At a point of PD that is exposed to illuminations ($= hc/q > E_g$), multiple e^-–h^+ pairs develop and electrons may recombine. However, photocurrent increases because of the higher field at the contact region, since the lighting effect decreases the electro-–hole pair recombination.[43] Sensor development and manufacturing that are sensitive to visible light and/or its near-infrared radiation (UV or NIR) are becoming essential for autonomous systems and instruments that are becoming more prevalent in our daily lives.

Due to this need, the PVP:Gr-$ZnTiO_3$ nanocomposite is used as an interfacial layer in PDs in the present study. Compared to traditional methods, the microwave-assisted process provides more homogeneous coating and deposition control, and this is how the interface layer was made. In the dark and upon illumination in the power range 40–100 mW cm^{-2}, the I–V measurement of the produced structures of Al/p-Si (MS) and Al/PVP:Gr-$ZnTiO_3$/p-Si (MPS) is performed at certain voltage ranges (± 3 V). For dark and illumination intensity, the constructed PDs resistance–voltage (R_i versus V) and N_{ss} versus (E_{ss}–E_v) plots are obtained from the I–V data at room temperature (RT). Moreover, the relation between the photocurrent with the light intensity is examined. At last, various photodetector properties including S, R, and D^* of the prepared structures are calculated and compared with each other and with the Al/PVP:$ZnTiO_3$/p-Si PD introduced in ref. [45]. The findings are thoroughly analyzed and compared to the PDs that are already represented in the literature.

2. Experimental Section

$TiCl_4$ (99%) and $Zn(CH_3COO)_2 \cdot 2H_2O$ (99%) were provided by ROYALEX and Merck Companies, respectively. We prepared TiO_2 nanopowders, as reported in our published research.[39] Before commencing the creation of $ZnTiO_3$ nanoparticles, we first produced 20 mL of TiO_2 (0.1 M), NaOH (0.2 M), and

$Zn(CH_3CO_2)_2$ (0.2 M) solutions in separate beakers. The first two solutions were gradually added to the last solution while it was at RT and exposed to ultrasonic radiation. After that, the results were placed inside a microwave and exposed to 800 W of radiation for 10 min. The product was then washed under centrifugation and dried at RT. Finally, the resulting nanoparticle was heated to 700 °C for 120 s. **Figure 1** shows the schematic of the preparation procedure of the $ZnTiO_3$ nanoparticles. To make the (PVP:Gr-ZnTiO₃) nanocomposite, 0.1 g $ZnTiO_3$ and 0.05 g graphene (Gr) nanoparticles were combined with 10 cc of PVP solution under ultrasonic radiation.

In this investigation, MS structures with/without (PVP:Gr-ZnTiO₃) interlayer were grown onto the same p-Si (B-doped) wafer that had a single-side polish, a thickness of ≈300 μm, an orientation of (100), a diameter of 2″, and a resistivity of 1–10 Ω cm. In order to clear any native oxide layer from the wafer's surface, this wafer was first ultrasonically cleaned for 5 min in a chemical solution of ($HF + 10H_2O$) before being cleaned with deionized water (DW). It was then cleaned in the chemical solutions of (H_2SO_4:H_2O_2:H_2O) with (5:1:1) and (HCl:H_2O) with (1:1) ratios for 4 min. Following that, it was adopted in high-purity DW with an 18 MΩ cm⁻¹ resistivity and dried with high-purity nitrogen (N_2) gas. Second, to achieve excellent or low-resistivity back Ohmic contact, the entire rear part of the wafer was thermally evaporated by high-pure Al (99.999%) at 150 nm thickness at 1 μTorr and then annealed at 500 °C for 5 min in N_2 environment.

Third, the (PVP:Gr-ZnTiO₃) solution was ready and spun onto the opposite or front side of the Si wafer at 3000 rpm for 1 min. The interlayer thickness (d_i) was estimated as 60 nm from the measured interlayer capacitance ($C_i = \varepsilon_i \varepsilon_0 A / d_i$). Finally, similar circular Schottky contacts of Al with a diameter of 1.0 mm and a thickness of 150 nm were also thermally evaporated onto the interlayer. A quartz metal thickness meter was used to control the Ohmic and rectifier metal contacts' thickness.

Both the schematic and energy band diagram of the Al/pSi (MS) and Al/(PVP:Gr-ZnTiO₃) (MPS) type PDs are schematically depicted in **Figure 2**. It should be mentioned that the I–V characteristics of the manufactured device were measured using a Keithley 4200 current/voltage source meter both in the dark and under various illumination intensities in a wide voltage range. Additionally, the MS and MPS-type PDs were exposed to illumination in the solar spectrum using a Newport-Oriel

69931, whose power ranges are 30–100 W cm⁻². A cooling fan was used to prevent the samples from heating under high illumination intensities.

3. Results and Discussion

Semilogarithmic I–V curves of the MS and MPS-type PDs in a voltage range (±3 V) and illumination powers (40–100 mW cm⁻²) are illustrated in **Figure 3**. The I–V profiles exhibit a linear behavior corresponding to the rectification effect at smaller positive voltages while deviating from linearity due to the presence of deposited (PVP:Gr-ZnTiO₃) interlayer, R_s, and N_{ss} because the applied voltage on the PD will be shared between of them and depletion layer. The thermionic emission (TE) theory is applied to study the performance of the constructed Si-based MS and MPS-PDs at the forward-bias region in the linear part of ln(I)–V plots both in dark and different illumination intensities. Thus, in this case where the structure has large enough R_s and n values are considerably deviated from unity ($n \geq 1$), the I–V relationship for the voltages greater than 3 (kT/q) is described as follows.[46–53]

$$I = I_0 \left[\exp\left(\frac{q(V_F - IR_s)}{nkT} \right) - 1 \right] \tag{1}$$

In Equation (1); the I_0, q, n, T, and IR_s quantities are the leakage/saturation current (I_0) at zero-bias voltage, electronic charge, quality/ideality factor (n), temperature in K, and voltage drop on R_s, respectively. The quantity of I_0 calculated by extrapolating the linear part of ln(I) versus V plot at zero-bias voltage is given as follows.[48]

$$I_0 = AA^* T^2 \exp\left(-\frac{q\varphi_{B0}}{kT} \right) \tag{2}$$

where A and A* are the rectifier-contact area of the diode and the Richardson constant. Therefore, the amount of I_0 is determined using the intersection point of the ln(I)–V curve for dark and each illumination intensity between 0.19 and 0.38 V. Thus, using the experimental value of I_0 and diode area (=7.85 × 10⁻³ cm²), the value of φ_{B0} was calculated as a function of illumination intensity like the other basic electrical parameters (I_0, n, and R_s).[48]

$$\varphi_{B0} = \frac{kT}{q} \ln\left(\frac{AA^* T^2}{I_0} \right) \tag{3}$$

The −1 value inside the square brackets (Equation 1) is small enough to be ignored compared to the exponential function next to it at room and above temperatures. Therefore, Equation (1) can be expressed as $\ln(I_F) = \ln(I_0) + d\ln(I_F)/dV_F$ for the linear part of $\ln(I_F)$ versus V_F plot. Thus, the value of n for MS and MPS-PDs was also calculated from the slope of ln(I)–V curves, $\tan\theta = d\ln(I)/dV$ as follows.[48,49]

$$n = \frac{q}{kT} \left(\frac{dV_F}{d\ln(I_F)} \right) \tag{4}$$

All these basic electrical parameters as a function of illumination power are shown in **Table 1**. When the fabricated PDs are
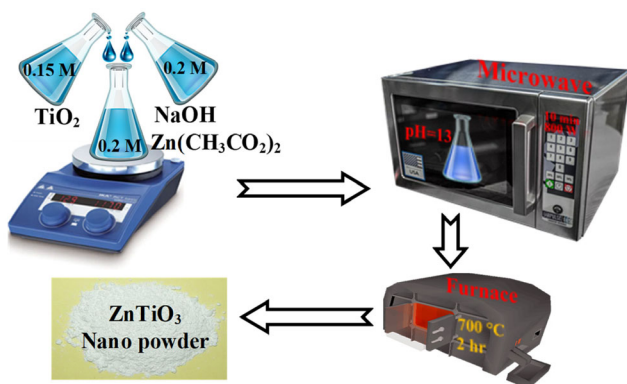

Figure 1. Schematic of the preparing procedure of $ZnTiO_3$ nanostructures.
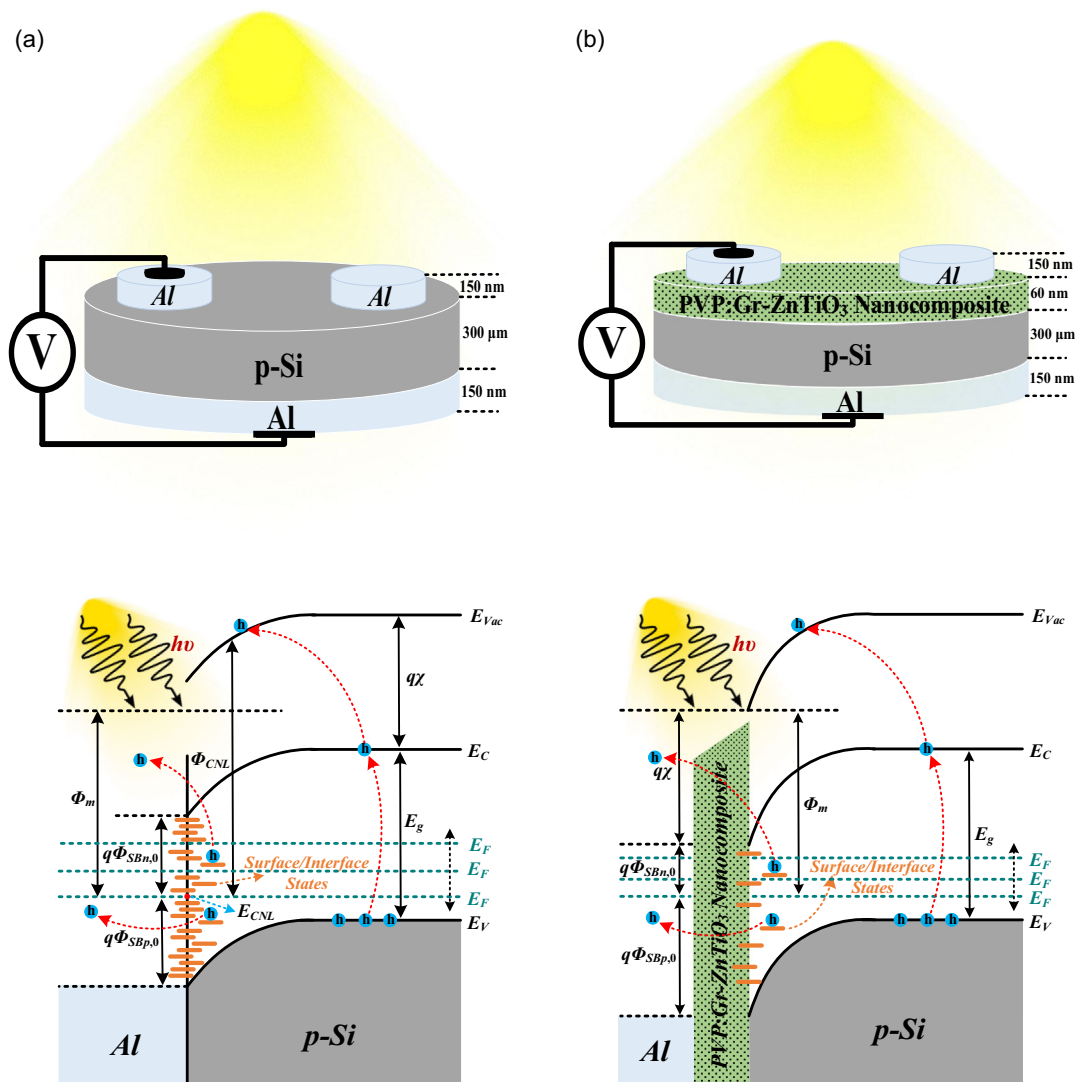
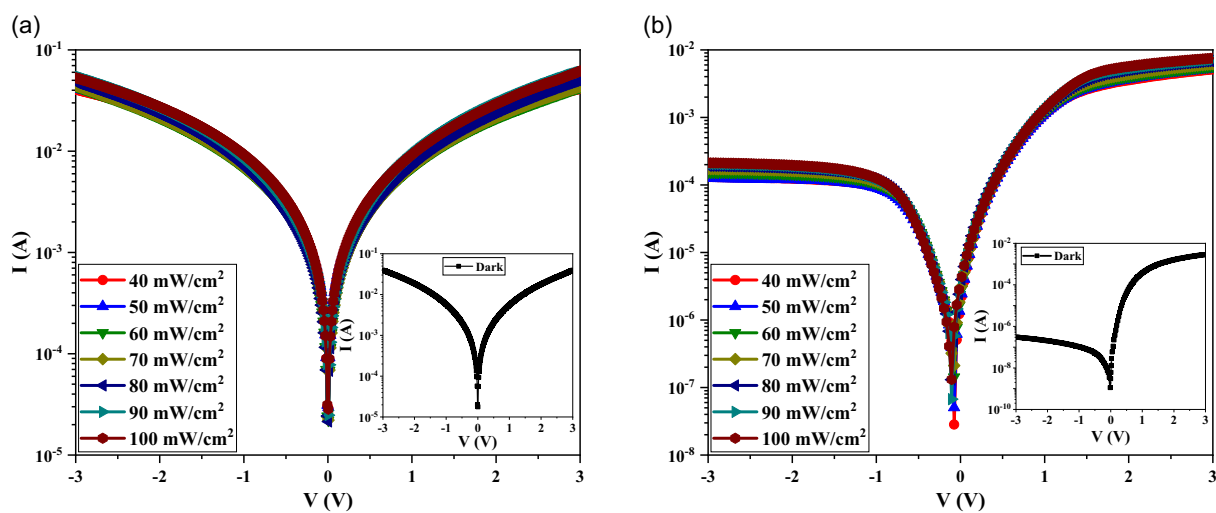**Figure 2.** Schematic of the a) MS- and b) MPS-type PDs with their energy-band diagrams under illumination.

Figure 3. The semilogarithmic plots of *I–V* values for the a) MS- and b) MPS-type PDs in the dark and under illumination.

Table 1. The illumination-dependent primary electronic parameters of the fabricated PDs calculated by TE theory.

PD	MS-type					MPS-type				
P [mW cm^{-2}]	I_o [μA]	Φ_{B0} [eV]	n	R_s [Ω]	R_{sh} [Ω]	I_o [μA]	Φ_{B0} [eV]	n	R_s [kΩ]	R_{sh} [kΩ]
0	74.26	0.591	2.55	76.05	75.87	0.08	0.768	2.75	1.04	9921
40	89.65	0.586	2.56	71.74	73.81	5.68	0.658	5.26	0.58	23.84
50	90.92	0.586	2.57	70.38	71.01	6.23	0.655	5.37	0.56	22.85
60	92.98	0.585	2.58	69.4	67.57	6.7	0.653	5.42	0.53	19.4
70	102.17	0.583	2.58	68.67	67.3	7.11	0.652	5.5	0.49	17.36
80	116.79	0.58	2.59	58.47	62.46	7.69	0.65	5.64	0.44	15.59
90	117.79	0.579	2.59	49.65	56.46	8.02	0.649	5.67	0.42	14.59
100	120.38	0.578	2.59	48.47	54.25	8.23	0.648	5.69	0.4	14.11

exposed to illumination, the value of I_0 increases from 74.26 and 0.08 μA and in dark conditions to 89.65 and 5.68 μA at the illumination power of 40 mW cm^{-2} for the MS- and MPS-type structures, respectively. This rise is continuing by the growing illumination power up due to the increment of photocurrent generated in the structures. The barrier height (BH) created at the M/S interface is also sensitive to light and starts to reduce for both structures after exposure to the light. Additionally, the n of the considered PDs increases with the light intensity. It is useful to mention that the quality of prepared PDs is represented by the value of n, which is expected to be nearly 1 at the ideal form. However, according to $[n = 1 + d_i/\varepsilon_s(\varepsilon_s/W_d + qN_{ss})]$, it may significantly deviate from the unity ($n = 1$, ideal case) in the usage because of several factors, including the presence of an interlayer thickness (d_i), and electric permittivity (ε_i), the dopant concentration of donor/acceptor atoms, the width of depletion layer (W_d), a specific N_{ss} distribution at the interface between the semiconductor and the interlayer, image-force lowering of the BH, production–recombination electrical charges, tunneling through interface states, and barrier nonuniformities at the interface between metal and semiconductor.[39,50,51]

The existence of N_{ss} with energies located in the bandgap of semiconductor acts as recombination centers, so they may capture/emit many electrons. The formation of an inhomogeneity of BH at the M/S interface is also more effective on the CCMs. The electrons do not have enough energy to pass over mean or higher BHs but can easily pass through these patches, leading to an increase in the current or ideality factor. Under external effects such as light and temperature, these traps become more effective in the CCMs because they have a special density distribution at the junction in the semiconductor bandgap due to the restructuring and reordering of electrons in these traps. Experimental results show that the use of a (PVP:Gr-ZnTiO$_3$) organic interfacial layer between Al and p-Si leads to an increase of BH, leakage current, and R_s when compared to MS diode. As shown in Figure 6, in dark, the interfacial traps are located between (0.1–0.51 eV) in the MS structure, while they are located deeper (0.45–0.73 eV) in the MPS structure. Therefore, in the MS structure, the charges in these traps can easily be excited to the valence band under light, while in the MPS structure, they transit between the traps rather than the valance band (E_v). This situation causes both the BH and the ideality

factor to change considerably with the illumination intensity in the MPS structure.

It should be noted that the R_s and R_{sh} quantities may also be found using the forward and reverse bias parts of the $I–V$ profiles. The efficiency or output of PDs and SCs is significantly impacted by these two features. Since the R_s and R_{sh} amounts relate to high-/low-enough forward and reverse bias, in turn, Ohm's law can be used to calculate how the resistance (R_i) of the structures increases in terms of voltage ($R_i = V_i/I_i$).[49] As a result, **Figure 4** shows the voltage dependence of R_i profiles for the produced MS- and MPS-PDs in the dark and under various illumination powers. This figure made it clear that when illumination power rose, photocurrent increased as well, which caused the R_s values to decrease. The variation of resistance in the structure without an interlayer is represented in Figure 4a. It is observed that $R_s \approx R_{sh}$, which can be attributed to the direct contact between the metal and the semiconductor interfaces, where both resistances arise from similar interface properties. Since the native SiO$_2$ insulator layer has not been completely removed in the washing process, the created photocurrent under illumination due to generation electron–hole pairs will be divided between the insulator layer, depletion layer of the diode, R_s, and surface states in the MS-type structure. In this case, the value of photocurrent becomes lower. It is clear that the native SiO$_2$ insulator layer cannot decrease the leakage current and passivated unwanted surface states. As expected, both the R_s and R_{sh} in the MPS-type structure decrease under illumination due to increase in the conductivity. Because many electrons (N_q) can be given the energy to stimulate from the E_v to the conduction band under illumination, as a result, the conductivity is enhanced ($\sigma = q\mu N_q = 1/\rho$).

The essential parameters of PDs (I_o, Φ_{B0}, n, and R_s/R_{sh}) are determined from the measurements and computations with TE theory as shown in Table 1. Based on common TE theory, it is supposed that the ideality factor is ideally equal to 1; therefore, a high amount of n implies a deviation from the TE hypothesis. In addition to n, the BH of the MS and MPS configurations might be a function of applied voltages at forward-bias region. Furthermore, the structure may include a lot of lower barriers or routes at mean BH, which would allow a lot of low-energy electrons to get through and raise the quantities of n and I_0. As shown in Table 1, the amounts of I_0 and n grow as the

**ADVANCED
SCIENCE NEWS**

www.advancedsciencenews.com

**ADVANCED
PHOTONICS
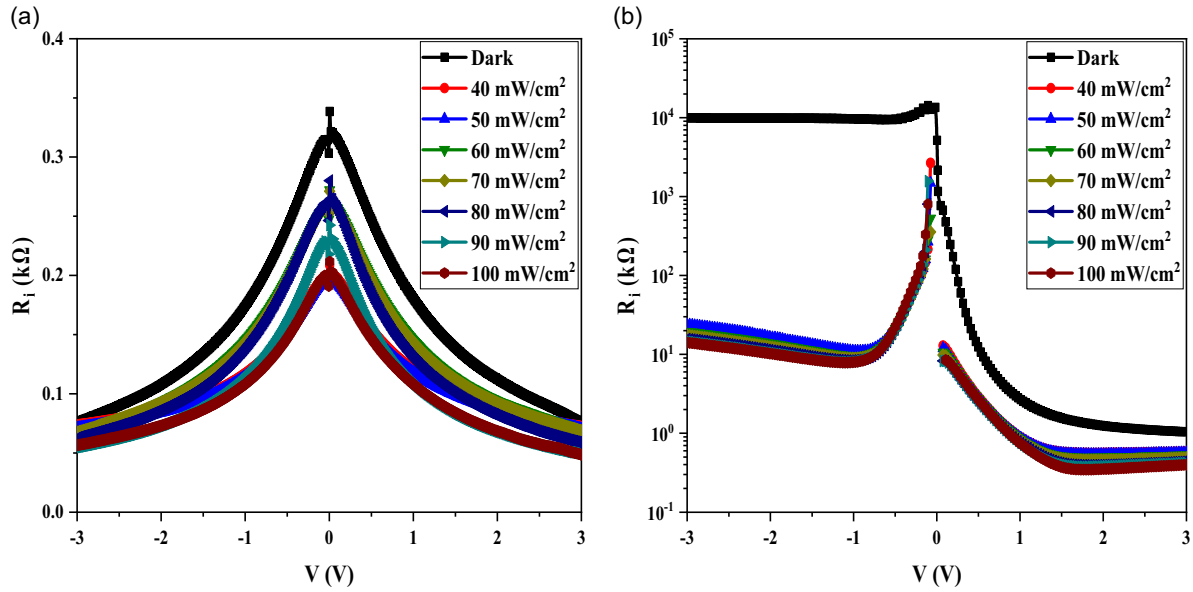RESEARCH**
Open Access

www.adpr-journal.com

Figure 4. The R_i–V curves of the a) MS- and b) MPS-type PDs in dark and under illumination conditions.

illumination intensity increases, whereas the quantities of Φ_{B0}, R_{sh}, and R_s decrease. This behavior is brought on by an increase in photocurrent in both voltage regions.

Several techniques, such as conventional TE theory and modified Norde function, may be used to identify the three most important electronic variables, Φ_{B0}, n, and R_s. However, each of these techniques corresponds to a different voltage region. Many mathematical techniques, including Ohm's law and modified Norde function, may be used to determine the true value of R_s from the forward bias I–V data; however, their properties may change depending on the selected or researched bias voltage. For instance, the Norde function is appropriate only in cases when the $\ln(I)$–V diagram has a distinct linear part, and Ohm's law states that larger forward-bias voltages are correlated with the true value of R_s in optoelectronic instruments.

Generally, the modified Norde method is used if the profiles of $\ln(I)$–V at the forward bias region do not have enough linear parts. According to another study,[52] the modified Norde technique's F(V) function for $n > 1$ is as follows.

$$F(V) = \frac{V}{\gamma} - \frac{kT}{q}\left[\ln\left(\frac{I(V)}{AA^*T^2}\right)\right] \qquad (5)$$

where γ stands for a positive dimensionless integer larger than n.

Using the amounts of V_{min} and I_{min}, which are taken from the F(V) functions (see **Figure 5**), it is possible to compute the Φ_{B0} and R_s contents as follows.[52]

$$\Phi_{B0} = F(V_{min}) + \frac{V_{min}}{\gamma} - \frac{kT}{q} \qquad (6a)$$

$$R_s = \frac{kT}{q}\frac{(\gamma - n)}{I_{min}} \qquad (6b)$$

Table 2 reports the two electrical features (Φ_{B0} and R_s) of the fabricated PDs based on the modified Norde function in the dark

and under different light intensities. As the illumination power increases, both quantities, Φ_{B0} and R_s, decrease. In addition, the findings produced using TE theory and the Norde function can be compared with each other. While the findings exhibit a good agreement, differences might be attributed to the distinct regions employed in these techniques to ascertain voltage-dependent characteristics. The observed discrepancies in the BH and R_s obtained from the Norde and TE models arise from the nature of the calculated method.

The optical response of the fabricated PDs is also more effectively affected by the presence of N_{ss} at the M/S interface, and this has a significant effect on the functionality and construction of electrical devices, such as SCs, MIS, and MPS PDs. Thus, using the following equations, which are extracted by the positive quantities of the electronic current and voltage and taken into account the Φ_{B0} and $n(V)$ depending on the applied voltage,[53] the energy-dependent variations of N_{ss} are computed as follows.

$$E_{ss} - E_v = (q\Phi_e - qV) \qquad (7a)$$

$$\Phi_e = \Phi_{B0} + \beta(V - IR_s) = \left(1 - \frac{1}{n(V)}\right)(V - IR_s) \qquad (7b)$$

$$N_{ss}(V) = \frac{\varepsilon_o}{q}\left[\frac{\varepsilon_i}{d_i}(n(V) - 1) - \frac{\varepsilon_s}{W_D}\right] \qquad (7c)$$

The interfacial layer thickness (d_i), the depletion layer width (W_D), the permittivity of the semiconductor (ε_s), and the permittivity of the interlayer (ε_i) are all parameters given in Equation (7a)–(7c). It should be noted that the estimation of the d_i and depletion width (W_D) is crucial for accurately determining the extracted interface states density. The interlayer thickness was calculated using capacitance–voltage (C–V) measurements, where the slope in the depletion region provided
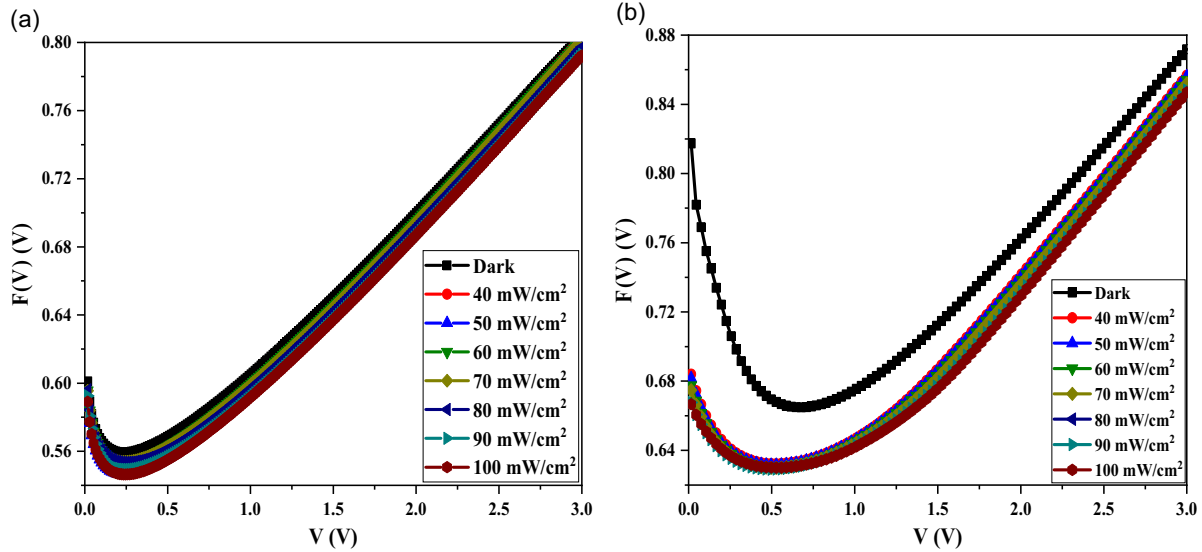
Figure 5. The variations of the $F(V)$–V curves of the a) MS- and b) MPS-type PDs at in the dark and under different illumination intensities.

Table 2. Two electronic variables (Φ_{B0} & R_s) of the prepared PDs in the dark and under illumination obtained by the modified Norde function.

PD	MS-type		MPS-type	
P [mW cm^{-2}]	Φ_{B0} [eV]	R_s [Ω]	Φ_{B0} [eV]	R_s [kΩ]
0	0.581	192.79	0.725	411.70
40	0.569	68.81	0.673	75.96
50	0.571	67.69	0.672	74.38
60	0.578	64.12	0.667	68.38
70	0.578	57.07	0.671	59.12
80	0.578	53.78	0.665	51.90
90	0.574	53.03	0.666	51.85
100	0.571	48.13	0.671	46.17

insights into the capacitance based on known dielectric properties. For the depletion width, we utilized the doping concentration obtained from previous characterization studies and determined the built-in potential from the C–V characteristics. These methodologies ensure that both parameters are reliably estimated, reflecting their significant influence on the interface states density.

The resulting value of N_{ss}, which is around $10^{13}/(eV\,cm^2)$ for the MS-type PD and $10^{12}/(eV\,cm^2)$ for the MPS PD, is shown as a function of energy for different illumination intensities in **Figure 6**. The observed discrepancies or locations in N_{ss} cause the resetting and reordering of the N_{ss} distribution under an illumination and an electric field. Figure 6 illustrates how the N_{ss} amounts effectively grow with illumination intensity, from near the semiconductor's middle bandgap toward the border of the E_v,
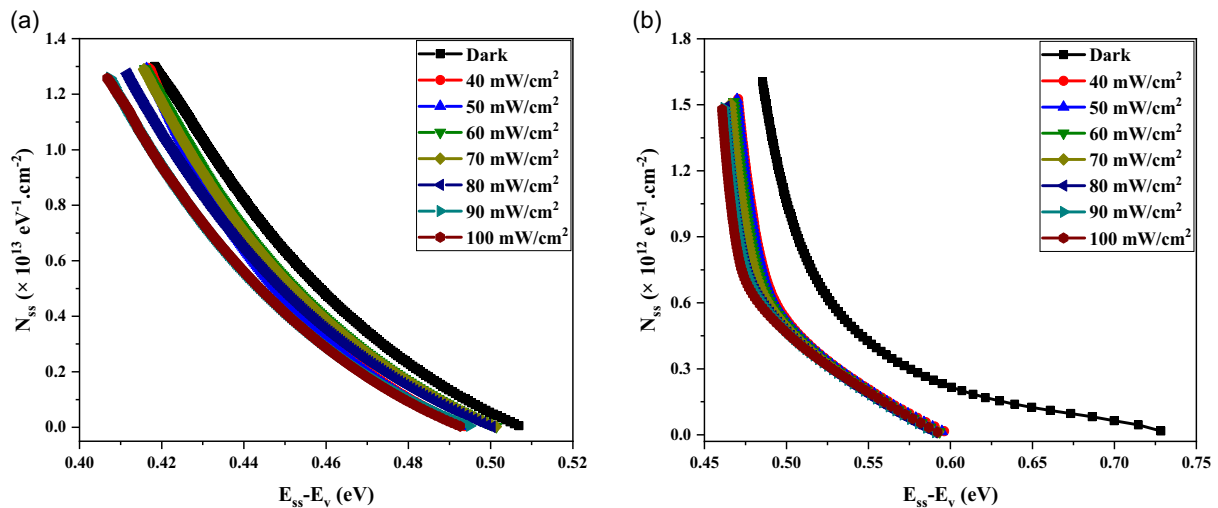

Figure 6. Variations of the interface states density in terms of energy for the a) MS and b) MPS PDs in the dark and under illumination.

**ADVANCED
SCIENCE NEWS**

www.advancedsciencenews.com

**ADVANCED
PHOTONICS
RESEARCH**
Open Access

www.adpr-journal.com

decreasing from 1.299×10^{13} to 1.394×10^{10}/(eV cm^2) for the reference structure (Figure 6a) and from 1.604×10^{12} to 1.019×10^{10}/(eV cm^2) for the MPS-type PD (Figure 6b).

This reduction is due to the reorganization and rearranging of the N_{ss} distribution under an illumination-induced electric field; the energy levels or traps are a center of $e^- -h^+$ recombination, absorbing and emitting electrons based on their lifetime and the intensity of the light. As a result, the illumination-induced interface/surface states can be reorganized and reconfigured upon an electric field, and their location moves to the top of the valance band. The presence of both R_s and N_{ss} is known to have a significant impact on the I–V characteristics of the MS and MPS PDs at forward bias. The sources of R_s are an Ohmic or rectifying junction, the probe wires used to the gate, the semiconductor bulk resistance, the atoms nonuniformly doped in the semiconductor, and the native/deposited thin film at the M/S interface.[50] The generation of N_{ss} is typically caused by the disruption of the periodic configuration of the semiconductor surface, surface preparation and cleaning, certain contaminants on the semiconductor, and organic contamination in the grown ambiance.[50]

On the other hand, the distribution of interface states, N_{ss} is primarily concentrated in the lower half of the silicon bandgap. This phenomenon can be attributed to several factors, including the presence of defects, impurities, and dislocations formed during fabrication processes, which create trap states that influence the electronic properties of the interface. Additionally, interactions between silicon and the insulating layers often lead to the formation of deeper energy states, further contributing to the predominance of interface states in this region. Understanding this distribution is essential, as it significantly impacts the performance of silicon-based devices.

The variations in the potential BH (Φ_{B0}) of the MS and MPS PDs in relation to light intensity (P) are depicted in **Figure 7**. As shown in Figure 7a, there is a link between Φ_{B0} and P in the reference structure, with the equation $\Phi_{B0}(P) = \Phi_{B0} - \alpha P = 0.593 + (-1.506 \times 10^{-4})P$ (eV). Moreover, the Φ_{B0} of the MPS PD depends on light intensity, with the equation $\Phi_{B0}(P) = \Phi_{B0} - \alpha P = 0.664 + (-3.423 \times 10^{-4})P$ (eV). The illumination

coefficient, represented by α in these equations, may be calculated as -1.506×10^{-4} and -3.423×10^{-4} for the MS- and MPS-type PDs, respectively. These values are near the negative temperature coefficient for the Si bandgap, which is -4.73×10^{-4} eV K^{-1}.[15] The dependence of the built-in Φ_{B0} on light power is a critical factor that reflects changes in carrier concentration and the associated thermal effects under varying illumination conditions. As light power increases, the generation of charge carriers enhances, influencing the potential barrier within the device and ultimately affecting its performance. The temperature coefficient is particularly relevant, as it describes how BH varies with temperature changes, which can be further influenced by the thermal energy associated with increased light power.[15]

Additionally, **Figure 8** illustrates how the Φ_{B0} of the fabricated PDs varies with n. As shown in Figure 8a, the equation $\Phi_{B0}(n) = (-0.228\,n + 1.170)$ eV indicates that Φ_{B0} and n are related in the MS-type PD. Furthermore, the ideal case value of Φ_{B0} for $n = 1$ is found to be 0.942 eV. In the case of the MPS PD, the value of Φ_{B0} changes in terms of n with an equation $\Phi_{B0}(n) = (-0.021\,n + 0.769)$ eV, which gives $\Phi_{B0} = 0.748$ eV at $n = 1$. It must be noted that several factors, including the thickness of the PVP:Gr-ZnTiO$_3$ thin film at the M/S interface, the depletion region width (W_d), the content of acceptor/donor atoms used as dopants (N_d), N_{ss}, and the nonuniformity of Φ_{B0}, cause the n values obtained for various illumination to be higher than 1.[54,55]

Figure 9 illustrates how photocurrent depends on light intensity in the manufactured MS- and MPS-type PDs. It is obvious that the photocurrent value increases with increasing light intensity. The data were fitted using the power law as follows.

$$I_{ph} \propto P^n \tag{8}$$

yielding a strong linear connection between photocurrent and light intensity, with power exponents of 0.48 and 0.87 for MS- and MPS-type PDs, respectively. The presence of trap states between the conduction band edge and the Fermi level led to an exponent value of less than 1 in the MS-type PD.[55] At the same time, they decreased by the PVP:Gr-ZnTiO$_3$ nanocomposite sandwiched
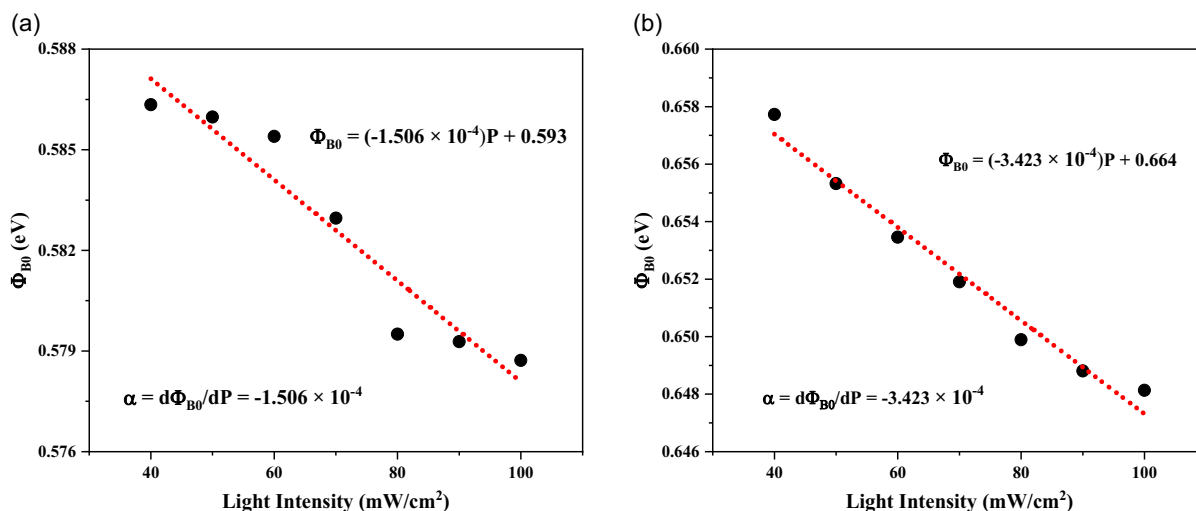

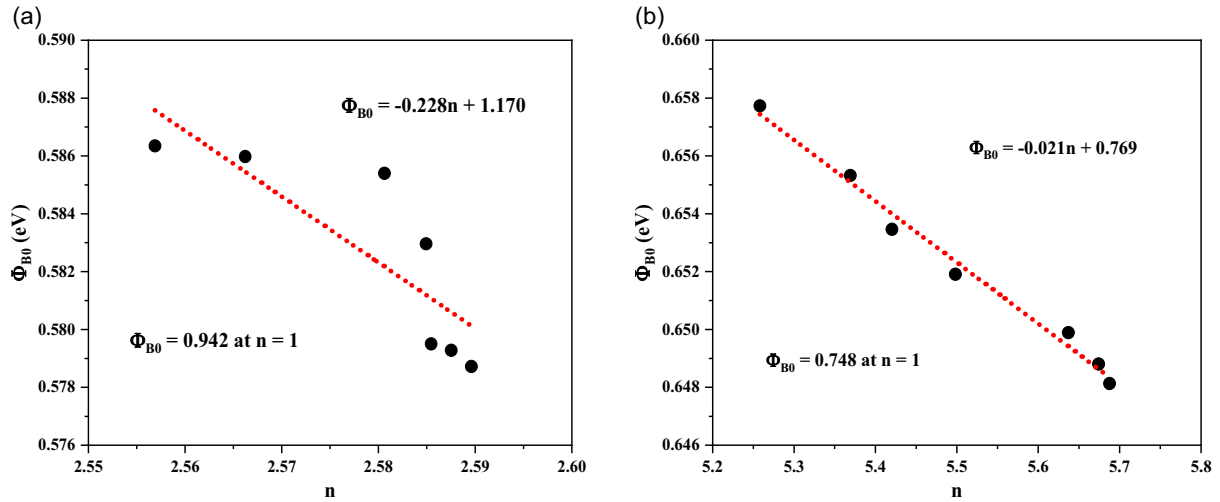**Figure 7.** The Φ_{B0}–P plots of the a) MS and b) MPS PDs.

ADVANCED
SCIENCE NEWS

www.advancedsciencenews.com

ADVANCED
PHOTONICS
RESEARCH
Open Access

www.adpr-journal.com

(a)

(b)

$\Phi_{B0} = -0.228n + 1.170$

$\Phi_{B0} = 0.942$ at $n = 1$

$\Phi_{B0} = -0.021n + 0.769$

$\Phi_{B0} = 0.748$ at $n = 1$

Figure 8. The Φ_{B0}–n profiles for the a) MS- and b) MPS-type PDs.

(a)

(b)

$I_{ph} \sim P^{0.48}$

$V_{bias} = 0$ V
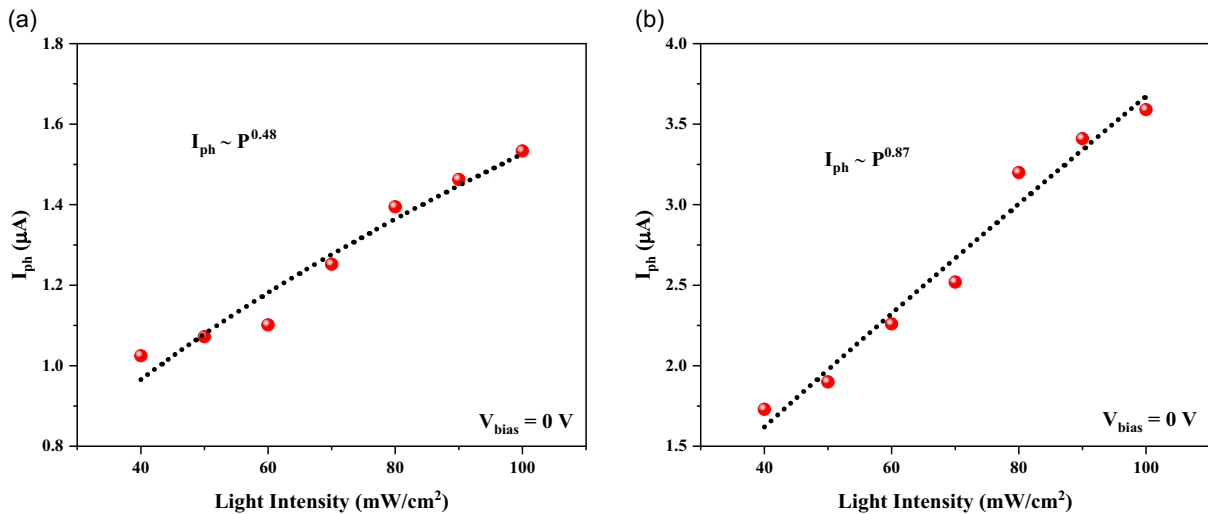
$I_{ph} \sim P^{0.87}$

$V_{bias} = 0$ V

Figure 9. The variations of I_{ph} versus light intensity for the a) MS and b) MPS PDs.

between metal and semiconductor layers; hence, this value increased to 0.87 for the MPS-type PD.

In the following, optical parameters of PDs, such as *S*, *R*, and *D**, are computed to examine the photodetecting performance to better understand the PD features under illumination. The photosensitivity of the PD is defined as the ratio of its dark to photoconductivities, which is given by[56]

$$S = \frac{I_{ph} - I_{dark}}{I_{dark}} \tag{9}$$

The value of *S* for the manufactured MS- and MPS-type PDs at the reverse bias, which ranges from −3 to 0 V, is shown in **Figure 10**. The results are presented with a reference structure (MS-type PD) to aid in understanding (see Figure 10a). The MPS PD with a structure of Al/PVP:Gr-ZnTiO₃/p-Si has a significant photosensitivity at the negative-bias region, as demonstrated in Figure 10b where the photosensitivity quantity grows as a

function of light intensity throughout all recorded reverse voltages. In the literature, similar findings for PDs with the MPS structure have recently been reported.[57–61] Compared to the PD described in studies,[58–60] the produced silicon-based PD provided in this study has a photosensitivity of around ≈1200, which is greater. Moreover, adding the graphene nanoparticles to the PVP:ZnTiO₃ nanocomposite remarkably improves the photosensitivity of the MPS-type PD compared with our previously publication,[45] which was equal to ≈500. It should be noted that a variety of factors, including the thickness of the interlayer, electric permittivity, nonuniform BH at the M/S interface, the interface states density (N_{ss}) distributed particularly at the semiconductor's bandgap, applied voltage dependency, and construction techniques, can influence the photosensitivity observed in PDs.

The ratio of the electric current relative to the optical power exposed to a PD gives the optical responsivity (*R*), which is expressed as[62]
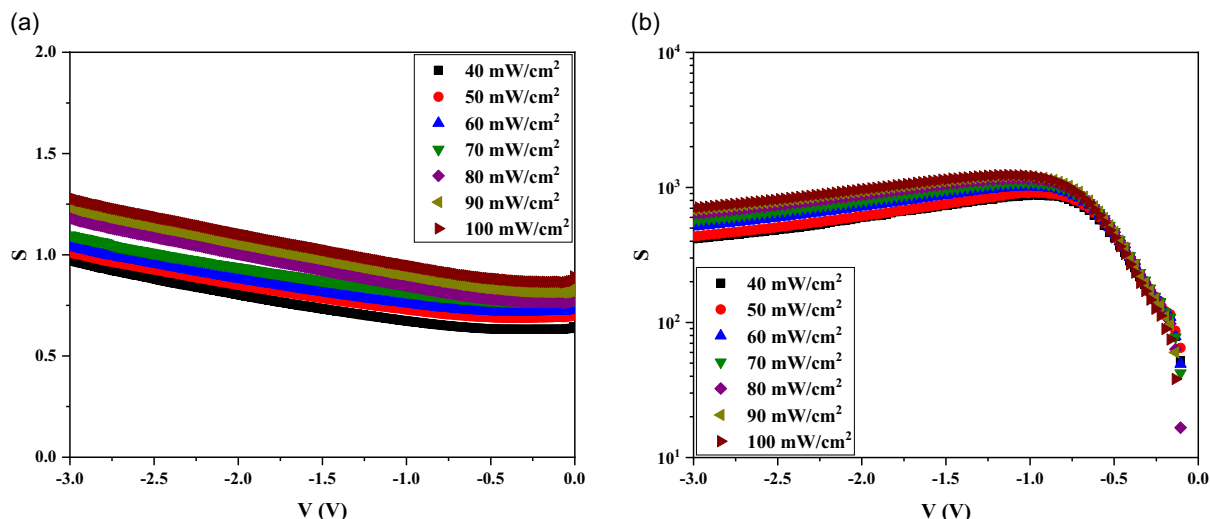
**ADVANCED
SCIENCE NEWS**

www.advancedsciencenews.com

**ADVANCED
PHOTONICS
RESEARCH**

www.adpr-journal.com

Figure 10. The S–V curves of the a) MS- and b) MPS-type PDs illuminated by different intensities.

$$R = \frac{I_{ph} - I_{dark}}{P_{Opt} \times A} \qquad (10)$$

where P_{Opt} denotes the power of the light illuminating on the PD surface (A) in $W\,cm^{-2}$. **Figure 11** displays the results of the optical responsivity for the MS- and MPS-type PDs that were determined at various illumination powers at the reverse bias region. As seen, the quantity of R increases with reducing light intensity and reached $0.06\ mA\,W^{-1}$ for the MS-type PD and $0.13\ mA\,W^{-1}$ for the MPS-type PD under a light intensity of $40\ mW\,cm^{-2}$ at 0 V, which is related to higher carrier recombination dynamics by increasing light intensity. Furthermore, a high value of R in the MPS-type PD is $400\ mA\,W^{-1}$ at a bias voltage of $-3\ V$, while this extreme value of R is equal to $125\ mA\,W^{-1}$ for the MS-type PD. Figure 11b demonstrates an approximately constant trend in optical responsivity with bias voltage in the MPS-type PD, which

is due to the activation of e^-–h^+ pairs generated by the incident light. However, it continuously decreases by the bias voltage in the MS-type PD (see Figure 11a). It is clear that the use of PVP: Gr-ZnTiO$_3$ nanocomposite significantly increases the optical responsivity of the MS-type PD. These findings are in good agreement with those reported by Yahia et al.[63] who demonstrated the device's suitability for photodiode/photosensor applications.

The most important parameter of merit for a photonic device is specific detectivity (D^*), which directly affects the sensitivity and performance of the detecting behavior of the device, especially in high-precision measurement and imaging applications that require the detection of weak signals. It is used to represent the photosensitivity of photonic devices such as photodiodes (PDs), solar cells (SCs), photosensors (PSs)/photodetectors (PDs), and is given by[64,65]
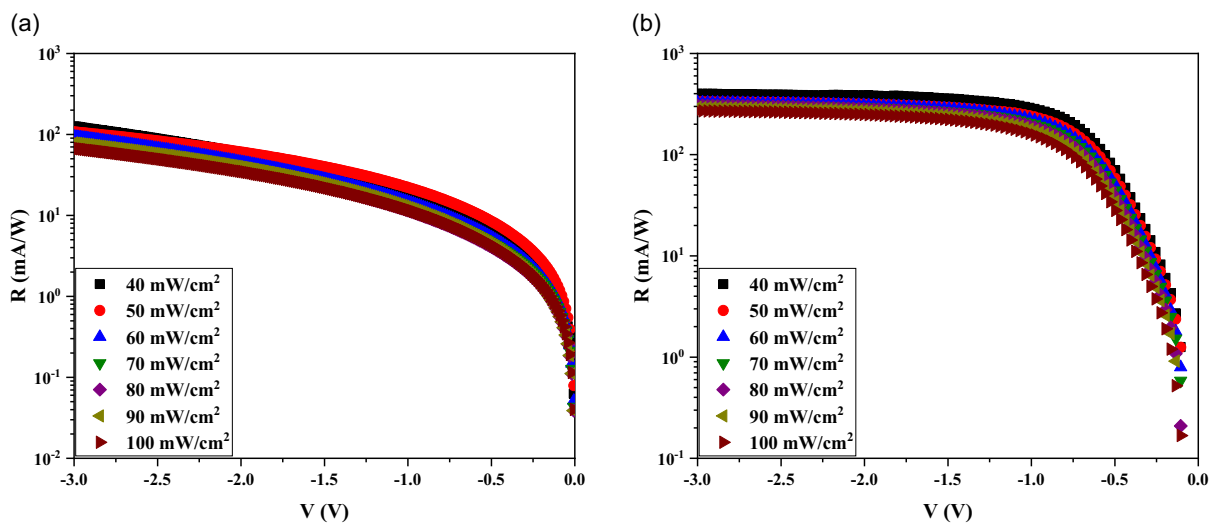

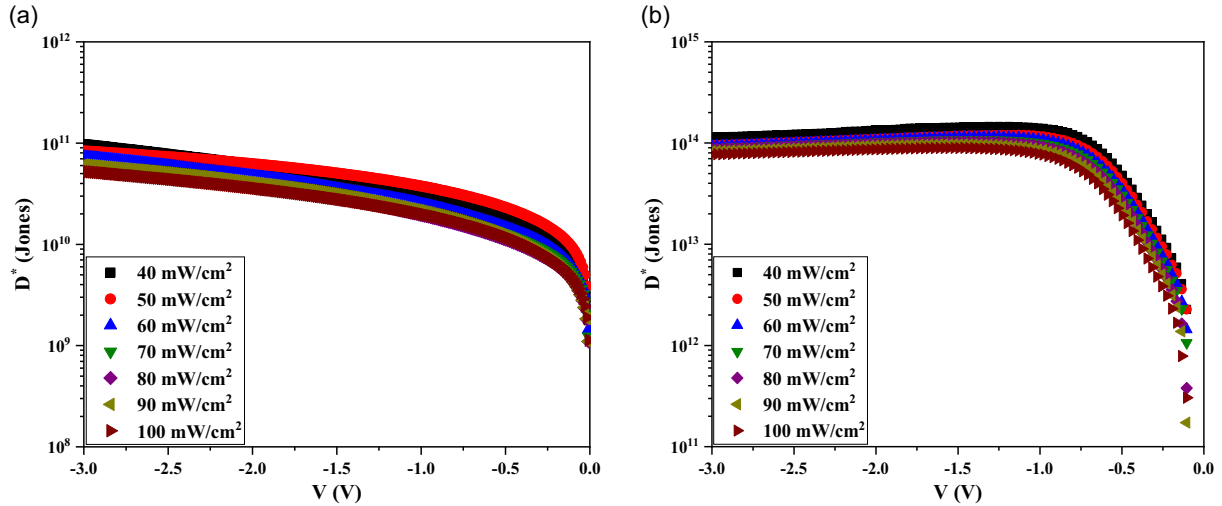**Figure 11.** The variations of R–V plots of the a) MS- and b) MPS-type PDs exposed by different intensities.

Figure 12. The changes of D–V graphs of the a) MS- and b) MPS-type PDs illuminated by different intensities.

$$D^* = R\sqrt{\frac{A}{2qI_{dark}}} = \frac{R}{I_n}\sqrt{A\Delta f} = \frac{1}{NEP}\sqrt{A\Delta f} \quad (11)$$

where I_n refers to the noise current, Δf denotes the noise bandwidth, and NEP stands for the noise equivalent power. On the other hand, the R, q, I_d, and A quantities are the photo or optic responsivity, dark current, electronic charge, and the effectively illuminated or rectifier contact area of the photonic device, respectively. The D^* is inversely proportional to the illumination intensity and decreases gradually with the increase in incident light density. That is, when the incident light intensity is low, the number of photogenerated electron–hole pairs is proportional to the number of incident photons. However, the number of photogenerated electron–hole pairs will be saturated with increasing light intensity, so the specific detection rate of them decreases nonlinearly. It is well known that only high-quality semiconductor crystals can suppress the dark current, resulting in high D^* photodetection performances. **Figure 12** shows the voltage-dependent D^* plotted against different light intensities for both PDs prepared in this work. The value of D^* increases with decreasing light intensity, and at zero-bias voltage, it reached 1.78×10^9 Jones (1 Jones $= 1$ cm $Hz^{1/2} W^{-1}$) for the MS-type PD and 2.25×10^{12} Jones for the MPS-type PD under a light intensity of 40 mW cm^{-2}, originating from the increment of recombination processes as the light intensity increases. It is also possible to see that a high D^* of 9.78×10^{10} Jones for the MS-type PD occurs at a bias voltage of -3 V, while a maximum D^* of 1.46×10^{14} Jones for the MPS PD is appeared at a bias voltage of -1.2 V.

The manufactured MPS PD shows strong photosensitivity at the negative-bias voltage, as seen by the progressive changes in S, R, and D^* values with the applied reverse voltages. These findings show that the PVP:Gr-ZnTiO$_3$ nanocomposite interlayer is more sensitive to light and that the diodes' sensitivity changes significantly with the bias voltage, compared to the PVP:ZnTiO$_3$ nanocomposite interfacial layer used by Barkhodari et al.[45] On the other hand, the density distribution of the trap levels (N_{ss}) at the structure–structure interface might be

considered the cause of the differences, including the peaks and fluctuations that show up in the voltage-dependent variations.[66,67] Furthermore, the drop in R and D^* values around zero bias is unmistakably linked to a decrease in photocurrent (0_{ph}), and the decrease in S values with rising reverse bias is coupled with an increase in dark current (I_{dark}).

4. Conclusion

In this study, using the spin-coating technique, a thin film with the composition of (PVP:Gr-ZnTiO$_3$) was utilized to create a PD rather than producing MS-type SDs utilizing an insulator layer produced by the traditional methods. Some important electric and optoelectronic parameters were then obtained by evaluating the I–V plots of the PDs subjected to illuminations within a range 40–100 mW cm^{-2} at RT. In order to ascertain the voltage dependency of the essential optoelectronic characteristics of the examined PDs at every power of illumination, the TE theory and modified Norde functions were used to acquire the Φ_{B0} and R_s and compared them. It was observed that as light power is increased, the amount of R_s and Φ_{B0} decreases while the value of n increases. Furthermore, measurements of the energy-dependent N_{ss} values were made in both dark and light conditions. Based on the results of the experiment, Φ_{B0}'s value decreases linearly as P and n increase. Specifically, the graphs of Φ_{B0}–P and Φ_{B0}–n yield the illumination coefficient ($\alpha = -1.506 \times 10^{-4}$ for the MS PD and $\alpha = -3.423 \times 10^{-4}$ for the MPS PD) and Φ_{B0} (0.942 eV for the MS PD and 0.748 eV for the MPS PD) at an ideal form ($n = 1$). Owing to the e$^-$–h$^+$ pairs that arise at the negative bias voltage due to growing illumination intensity, an increment of I_{ph} was also observed. The exponent values for the MS- and MPS-type PD were 0.48 and 0.87 due to the trap states formation between the valance band and the intrinsic level. The PVP:Gr-ZnTiO$_3$ nanocomposite at the M/S interface results in decreasing the trap states and hence, the exponent value increased. The Si-based MPS PD has a photosensitivity (S) of around 1200, an optical responsivity (R) of 400 mA W^{-1}, and a specific detectivity

of 1.46×10^{14} Jones, which is greater than the MS-type PD and other PDs reported in the literature. Based on these results, it is possible to use the fabricated MPS PD with a configuration of Al/PVP:Gr-ZnTiO$_3$/p-Si for applications in optoelectronic and photovoltaic devices.

Conflict of Interest

The authors declare no conflict of interest.

Author Contributions

Ali Barkhordari: conceptualization (lead); data curation (lead); formal analysis (lead); writing—original draft (lead). **Şemsettin Altındal**: supervision (equal); writing—review and editing (equal). **Süleyman Özçelik**: supervision (equal); writing—review and editing (equal). **Hamid Reza Mashayekhi**: supervision (equal); writing—review and editing (equal). **Mustafa Muradov**: supervision (equal); writing—review and editing (equal). **Yashar Azizian-Kalandaragh**: project administration (lead); supervision (equal); writing—review and editing (equal).

Data Availability Statement

The data that support the findings of this study are available from the corresponding author upon reasonable request.

Keywords

[1] H. Tomozawa, D. Braun, S. D. Phillips, R. Worland, A. J. Heeger, H. Kroemer, *Synth. Met.* **1989**, *28*, 687.

[2] D. Yang, D. Ma, *Adv. Opt. Mater.* **2019**, *7*, 1800522.

[3] S. Ying, Z. Ma, Z. Zhou, R. Tao, K. Yan, M. Xin, Y. Li, L. Pan, Y. Shi, *IEEE Access* **2020**, *8*, 189646.

[4] R. Yang, M. Benner, Z. Guo, C. Zhou, J. Liu, *Adv. Funct. Mater.* **2021**, *31*, 2103132.

[5] Y. Meng, X. Zhang, Y. Ma, X. Feng, *ACS Appl. Electron. Mater.* **2020**, *2*, 3577.

[6] B. Zhang, J. Liu, M. Ren, C. Wu, T. J. Moran, S. Zeng, S. E. Chavez, Z. Hou, Z. Li, A. M. LaChance, T. R. Jow, *Adv. Mater.* **2021**, *33*, 2101374.

[7] Y. Wang, S. Nasreen, D. Kamal, Z. Li, C. Wu, J. Huo, L. Chen, R. Ramprasad, Y. Cao, *ACS Appl. Mater. Interfaces* **2021**, *13*, 46142.

[8] J. Meng, Z. H. Guo, C. Pan, L. Wang, C. Chang, L. Li, X. Pu, Z. L. Wang, *ACS Energy Lett.* **2021**, *6*, 2442.

[9] P. Puneetha, S. P. Mallem, S. C. Park, S. Kim, D. H. Heo, C. M. Kim, J. Shim, S. J. An, D. Y. Lee, K. I. Park, *Nano Res.* **2023**, *16*, 5541.

[10] R. Gupta, S. C. Misra, B. D. Malhotra, N. N. Beladakere, S. Chandra, *Appl. Phys. Lett.* **1991**, *58*, 51.

[11] J. R. Cárdenas, E. A. de Vasconcelos, W. M. de Azevedo, E. F. da Silva, I. Pepe, A. F. da Silva, S. S. Ribeiro, K. A. Silva, *Appl. Surf. Sci.* **2008**, *255*, 688.

[12] Y. Hu, J. Zhou, P. H. Yeh, Z. Li, T. Y. Wei, Z. L. Wang, *Adv. Mater.* **2010**, *22*, 3327.

[13] X. Zhou, D. Yang, D. Ma, *Adv. Opt. Mater.* **2015**, *3*, 1570.

[14] A. Islam, J. Li, M. Pervaiz, Z. H. Lu, M. Sain, L. Chen, X. Ouyang, *Adv. Energy Mater.* **2019**, *9*, 1803354.

[15] S. M. Sze, Y. Li, K. K. Ng, in *Physics of Semiconductor Devices*, John Wiley & Sons, New York **2021**.

[16] S. Bel, C. Lobre, S. Petit, M. Veillerot, G. Badano, *J. Electron. Mater.* **2024**, 1.

[17] H. Águas, A. Goullet, L. Pereira, E. Fortunato, R. Martins, *Thin Solid Films* **2004**, *451*, 361.

[18] N. Wang, X. Li, Y. Wang, Y. Hou, X. Zou, G. Chen, *Mater. Lett.* **2008**, *62*, 3691.

[19] B. B. Rao, *Mater. Chem. Phys.* **2000**, *64*, 62.

[20] Y. Yoshino, T. Makino, Y. Katayama, T. Hata, *Vacuum* **2000**, *59*, 538.

[21] S. Jäger, B. Szyszka, J. Szczyrbowski, G. Bräuer, *Surf. Coat. Technol.* **1998**, *98*, 1304.

[22] R. W. Birkmire, E. Eser, *Annu. Rev. Mater. Sci.* **1997**, *27*, 625.

[23] D. C. Look, *Mater. Sci. Eng., B* **2001**, *80*, 383.

[24] A. B. Bodade, A. M. Bende, G. N. Chaudhari, *Vacuum* **2008**, *82*, 588.

[25] X. Zhang, F. Zhang, K. Y. Chan, *Mater. Chem. Phys.* **2006**, *97*, 384.

[26] H. T. Kim, S. Nahm, J. D. Byun, K. Y. Low-Fired, *J. Am. Ceram. Soc.* **1999**, *82*, 3476.

[27] H. Obayashi, Y. Sakurai, T. Gejo, *J. Solid State Chem.* **1976**, *17*, 299.

[28] Y. Shimizu, H. Komatsu, S. Michishita, N. Miura, N. Yamazo, *Sens. Actuators, B* **1996**, *34*, 493.

[29] A. Barkhordari, H. Mashayekhi, P. Amiri, Ş. Altındal, Y. Azizian-Kalandaragh, *Appl. Phys. A* **2023**, *129*, 249.

[30] M. Gabrovska, R. Edreva-Kardjieva, K. Tenchev, P. Tzvetkov, A. Spojakina, L. Petrov, *Appl. Catal., A* **2011**, *399*, 242.

[31] Y. Gui, S. Li, J. Xu, C. Li, *Microelectron. J.* **2008**, *39*, 1120.

[32] S. F. Wang, F. Gu, M. K. Lü, C. F. Song, D. Xu, D. R. Yuan, S. W. Liu, *Chem. Phys. Lett.* **2003**, *373*, 223.

[33] A. Barkhordari, H. R. Mashayekhi, P. Amiri, Ş. Altındal, Y. Azizian-Kalandaragh, *Semicond. Sci. Technol.* **2023**, *38*, 075002.

[34] U. Steinike, B. Wallis, *Cryst. Res. Technol.* **1997**, *32*, 187.

[35] Y. S. Chang, Y. H. Chang, I. G. Chen, G. J. Chen, Y. L. Chai, T. H. Fang, *Ceram. Int.* **2004**, *30*, 2183.

[36] A. Barkhordari, H. R. Mashayekhi, P. Amiri, S. Özçelik, Ş. Altındal, Y. Azizian-Kalandaragh, *Sci. Rep.* **2023**, *13*, 13685.

[37] Z. Durmus, A. Durmus, H. Kavas, *J. Mater. Sci.* **2015**, *50*, 1201.

[38] P. Avouris, *Nano Lett.* **2010**, *10*, 4285.

[39] A. Barkhordari, S. Özçelik, Ş. Altındal, G. Pirgholi-Givi, H. Mashayekhi, Y. Azizian-Kalandaragh, *Phys. Scr.* **2021**, *96*, 085805.

[40] H. J. Son, L. Lu, W. Chen, T. Xu, T. Zheng, B. Carsten, J. Strzalka, S. B. Darling, L. X. Chen, L. Yu, *Adv. Mater.* **2013**, *25*, 838.

[41] T. A. Shastry, I. Balla, H. Bergeron, S. H. Amsterdam, T. J. Marks, M. C. Hersam, *ACS Nano* **2016**, *10*, 10573.

[42] R. Shanti, F. Bella, Y. S. Salim, S. Y. Chee, S. Ramesh, K. Ramesh, *Mater. Design* **2016**, *108*, 560.

[43] I. M. Ashraf, A. A. El-Zahhar, *Results Phys.* **2018**, *11*, 842.

[44] J. H. Park, T. W. Lee, B. D. Chin, D. H. Wang, O. O. Park, *Macromol. Rapid Commun.* **2010**, *31*, 2095.

[45] A. Barkhordari, H. R. Mashayekhi, P. Amiri, Ş. Altındal, Y. Azizian-Kalandaragh, *Opt. Mater.* **2024**, *148*, 114787.

[46] L. Hou, Y. D. Hou, M. K. Zhu, J. Tang, J. B. Liu, H. Wang, H. Yan, *Mater. Lett.* **2005**, *59*, 197.

[47] A. Barkhordari, S. Özçelik, G. Pirgholi-Givi, H. R. Mashayekhi, Ş. Altındal, Y. Azizian-Kalandaragh, *Silicon* **2022**, *14*, 5437.

[48] Y. Azizian-Kalandaragh, A. Barkhordari, S. Özçelik, Ş. Altındal, *Phys. Scr.* **2024**, *99*, 086001.

[49] A. Barkhordari, Ş. Altındal, G. Pirgholi-Givi, H. Mashayekhi, S. Özçelik, Y. Azizian-Kalandaragh, *Silicon* **2023**, *15*, 855.

**ADVANCED
SCIENCE NEWS**

www.advancedsciencenews.com

**ADVANCED
PHOTONICS
RESEARCH**
Open Access

www.adpr-journal.com

[50] E. H. Nicollian, J. R. Brews, in *MOS (Metal Oxide Semiconductor) Physics and Technology*, John Wiley & Sons, New York **2002**.

[51] Ş. Altındal, A. Barkhordari, S. Özçelik, G. Pirgholi-Givi, H. R. Mashayekhi, Y. Azizian-Kalandaragh, *Phys. Scr.* **2021**, *96*, 125838.

[52] H. Norde, *J. Appl. Phys.* **1979**, *50*, 5052.

[53] H. C. Card, E. H. Rhoderick, *J. Phys. D: Appl. Phys.* **1971**, *4*, 1589.

[54] M. O. Erdal, M. Yıldırım, A. Kocyigit, *J. Mater. Sci.: Mater. Electron.* **2019**, *30*, 13617.

[55] İ. Dökme, S. Altindal, İ. Uslu, *J. Appl. Polym. Sci.* **2012**, *125*, 1185.

[56] A. Dere, B. Coskun, A. D. Tataroğlu, A. G. Al-Sehemi, A. A. Al-Ghamdi, H. M. Alateeq, R. Qindeel, W. A. Farooq, F. Yakuphanoglu, *Phys. B: Condens. Matter* **2018**, *545*, 86.

[57] A. Yeşildağ, M. Erdoğan, Ö. Sevgili, Z. Çaldıran, İ. Orak, *J. Electron. Mater.* **2021**, *50*, 6448.

[58] M. O. Erdal, A. Kocyigit, M. Yıldırım, *Chin. J. Phys.* **2020**, *64*, 163.

[59] S. Khalili, H. M. Chenari, F. Yıldırım, Z. Orhan, S. Aydogan, *J. Alloys Compd.* **2021**, *889*, 161647.

[60] A. M. El-Mahalawy, M. A. Salam, *Appl. Phys. A* **2020**, *126*, 393.

[61] B. Gündüz, N. Turan, E. Kaya, N. Colak, *Synth. Met.* **2013**, *184*, 73.

[62] L. C. Chen, M. I. Lu, *Scr. Mater.* **2009**, *61*, 781.

[63] I. S. Yahia, A. A. Farag, R. Jafer, J. Iqbal, H. Y. Zahran, S. Chusnutdinow, T. Wojtowicz, K. G. Electrical, *Mater. Sci. Semicond. Process.* **2017**, *67*, 33.

[64] R. Zhuo, L. Zeng, H. Yuan, D. Wu, Y. Wang, Z. Shi, T. Xu, Y. Tian, X. Li, Y. H. Tsang, *Nano Res.* **2019**, *12*, 183.

[65] E. Wu, D. Wu, C. Jia, Y. Wang, H. Yuan, L. Zeng, T. Xu, Z. Shi, Y. Tian, X. Li, *ACS Photonics* **2019**, *6*, 565.

[66] S. O. Tan, H. Uslu Tecimer, O. Çiçek, H. Tecimer, I. Orak, Ş. Altındal, *J. Mater. Sci.: Mater. Electron.* **2016**, *27*, 8340.

[67] Ç. Güçlü, E. E. Tanrıkulu, A. Dere, Ş. Altındal, Y. Azizian-Kalandaragh, *J. Mater. Sci.: Mater. Electron.* **2023**, *34*, 1909.

2400171 (13 of 13)